catalysts

MDPI

Article

Study on Thermal Decomposition Behavior, Gaseous Products, and Kinetic Analysis of Bis-(Dimethylglyoximato) Nickel(II) Complex Using TG-DSC-FTIR-MS Technique

Ergang Yao [1], Siyu Xu [1], Fengqi Zhao [1,*], Taizhong Huang [2], Haijian Li [1], Ningning Zhao [3], Jianhua Yi [1], Yanjing Yang [1] and Changjian Wang [1]

1 Science and Technology on Combustion and Explosion Laboratory, Xi'an Modern Chemistry Research Institute, Xi'an 710065, China; yaoerg@126.com (E.Y.); xusy99@163.com (S.X.); h.j.Li@outlook.com (H.L.); npecc_yjh2819@163.com (J.Y.); mseyyj@163.com (Y.Y.); workhard@163.com (C.W.)

2 Key Laboratory of Chemical Sensing & Analysis in Universities of Shandong, School of Chemistry and Chemical Engineering, University of Jinan, Jinan 250022, China; chm_huangtz@ujn.edu.cn

3 School of Science, Xi'an University of Technology, Xi'an 710054, China; zhaonn@xaut.edu.cn

* Correspondence: npecc@163.com; Tel.: +86-029-8829-1663

Received: 27 February 2020; Accepted: 13 March 2020; Published: 15 March 2020

Abstract: The fiber-like bis-(dimethylglyoximato) nickel(II) complex, $Ni(DMG)_2$ was successfully synthesized. The obtained samples were characterized by SEM-EDS, FT-IR, XRD, and XPS. The TG-DSC-FTIR-MS coupling technique was used to characterize the thermal decomposition behavior and evolved gas analysis of $Ni(DMG)_2$. The non-isothermal decomposition reaction kinetic parameters were obtained by both combined kinetic analysis and isoconversional Vyazovkin methods. It was found that $Ni(DMG)_2$ begins to decompose at around 280 °C, and a sharp exothermic peak is observed in the DSC curve at about 308.2 °C at a heating rate of 10 °C·min^{-1}. The main gaseous products are H_2O, NH_3, N_2O, CO, and HCN, and the content of H_2O is significantly higher than that of the others. The activation energy obtained by the combined kinetic analysis method is 170.61 ± 0.65 kJ·mol^{-1}. The decomposition process can be described by the random nucleation and growth of the nuclei model. However, it was challenging to attempt to evaluate the reaction mechanism precisely by one ideal kinetic model.

Keywords: nickel (II) complex; dimethylglyoxime; thermal behavior; kinetic analysis; combustion catalyst

1. Introduction

Combustion catalysts, as one of the main ingredients, play an essential role in the modification of the burning rate and combustion stability of solid propellants [1–3]. A variety of combustion catalysts, such as transition metal oxides (e.g., CuO, PbO, NiO) [4–8], compounds (e.g., lead salicylate, copper adipate, copper salicylate) [9–11], and nano-metal particles (e.g., Ni, Bi) [12–14], have been up to now studied extensively. In the combustion process of solid propellants, the combustion catalyst acts as a heterogeneous catalyst, and its catalytic activity primarily depends on its active sites. Generally, the selection principle and method of the combustion catalyst are their catalytic activity and energy.

Although transition metal oxides such as NiO are a class of high-efficiency combustion catalysts for solid propellants and have excellent catalytic effect [15], they have no contribution to the combustion except for their catalytic effect. With the requirement to further enhance the burning rate, it is usually required to add more catalyst. Then the energy property of the solid propellants decreases because

of a large amount of transition metal oxides, which cannot release any energy during combustion. Therefore, developing new energetic burning catalysts to increase the burn rate and reduce energy losses is crucial for the solid propellant. This problem could be overcome by using energetic combustion catalysts, in which an exothermic effect can be generated during the decomposition and combustion process of the propellants [16].

Bis-(dimethylglyoximato) nickel(II) complex, $Ni(DMG)_2$, is usually synthesized by the reaction of dimethylglyoxime and Ni^{2+} cations. This reaction has been much used to detect and estimate the presence of Ni in solution [17,18]. For the $Ni(DMG)_2$ complex, the thermal decomposition reaction is a rapid exothermic reaction, which produces a lot of heat during the process. Additionally, the main thermolysis products of $Ni(DMG)_2$ complex are NiO and carbon [19–21]. NiO by this method of formation in-situ usually has a higher catalytic activity than the direct addition of NiO. The carbon framework formed by the thermal decomposition of $Ni(DMG)_2$ complex can also increase the dispersion of NiO species on the burning surface of solid propellants, and then the catalytic efficiency of NiO can be further improved. Thus, the $Ni(DMG)_2$ complex can be used as a new type of energetic burning catalysts that not only enhances the burning rate, but also results in a low energy loss to the solid propellant system.

As is known, the thermal decomposition behavior of combustion catalysts has a significant effect on the catalytic property of combustion. The studies of the structure, decomposition kinetics, and thermal behaviors are very important for the selection and application of new combustion catalysts. Some of the previous studies on thermal decomposition reaction of $Ni(DMG)_2$ complex were mainly focused on the different properties of NiO nanoparticles, which were obtained by the thermal pyrolysis of the $Ni(DMG)_2$ precursor [19,21]. However, the correlation study between the thermal decomposition mechanism, the formation of gas products, and the reaction kinetics of $Ni(DMG)_2$ complex has been scarcely reported.

The main objective of this paper is to investigate the thermal decomposition reaction behavior and non-isothermal decomposition reaction kinetics of the $Ni(DMG)_2$ complex. The reaction models and kinetic parameters obtained by combined kinetic analysis and isoconversional Vyazovkin methods are also reported.

2. Results and Discussion

2.1. Morphology and Structure Characterization

Figure 1a,b represents the SEM images of the as-prepared $Ni(DMG)_2$ complex. It can be seen from Figure 1 that the surface morphology of the $Ni(DMG)_2$ is a nanofiber-like structure with different lengths, the average diameter is about 200 nm, and the fibers are in close proximity to each other. EDS is used to analyze the element types and the relative contents of atoms. The EDS image of $Ni(DMG)_2$ complex (Figure 1d) shows that the peaks of C, O, N, and Ni elements are present. The contents of C, O, N, and Ni elements are about 31.95%, 26.05%, 19.51%, and 22.49%.

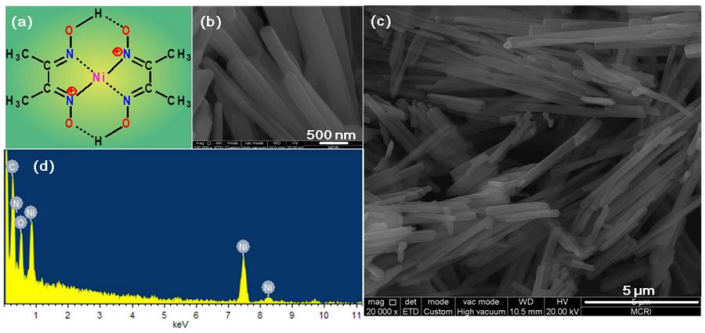

Figure 1. (**a**) Chemical structure of the bis-(dimethylglyoximato) nickel(II) complex ($Ni(DMG)_2$) molecule. (**b**,**c**) SEM images and (**d**) EDS spectra of the $Ni(DMG)_2$ complex.

$Ni(DMG)_2$ complex was dried under vacuum for 2 h, and its XRD pattern is shown in Figure 2a. The very narrow and sharp high-intensity diffraction peak of the diffraction pattern with a preferentially exposed (110) plane at 2θ of 10.0°, indicates a highly crystalline structure. The average grain size calculated by the Debye-Scherrer formula based on the most intense (110) diffraction peak was about 125.0 nm. The remaining peaks of $Ni(DMG)_2$ observed at the 2θ values of 10.63, 19.35, 26.13, 27.52, 28.17, 29.36, 32.61, 34.87, 36.05, 38.92, 43.67, and 46.08° can be assigned as the (200), (211), (130), (002), (510), (112), (022), (521), (240), (710), (150), and (242) planes, respectively [22–25]. From the diffraction pattern in Figure 2a, $Ni(DMG)_2$ is attributed to the orthorhombic system, *Ibam* space group with a = 16.575 Å, b = 10.423 Å, c = 6.474 Å and $\alpha = \beta = \gamma$ = 90° [26–29], which confirms the good chemical purity of the materials.

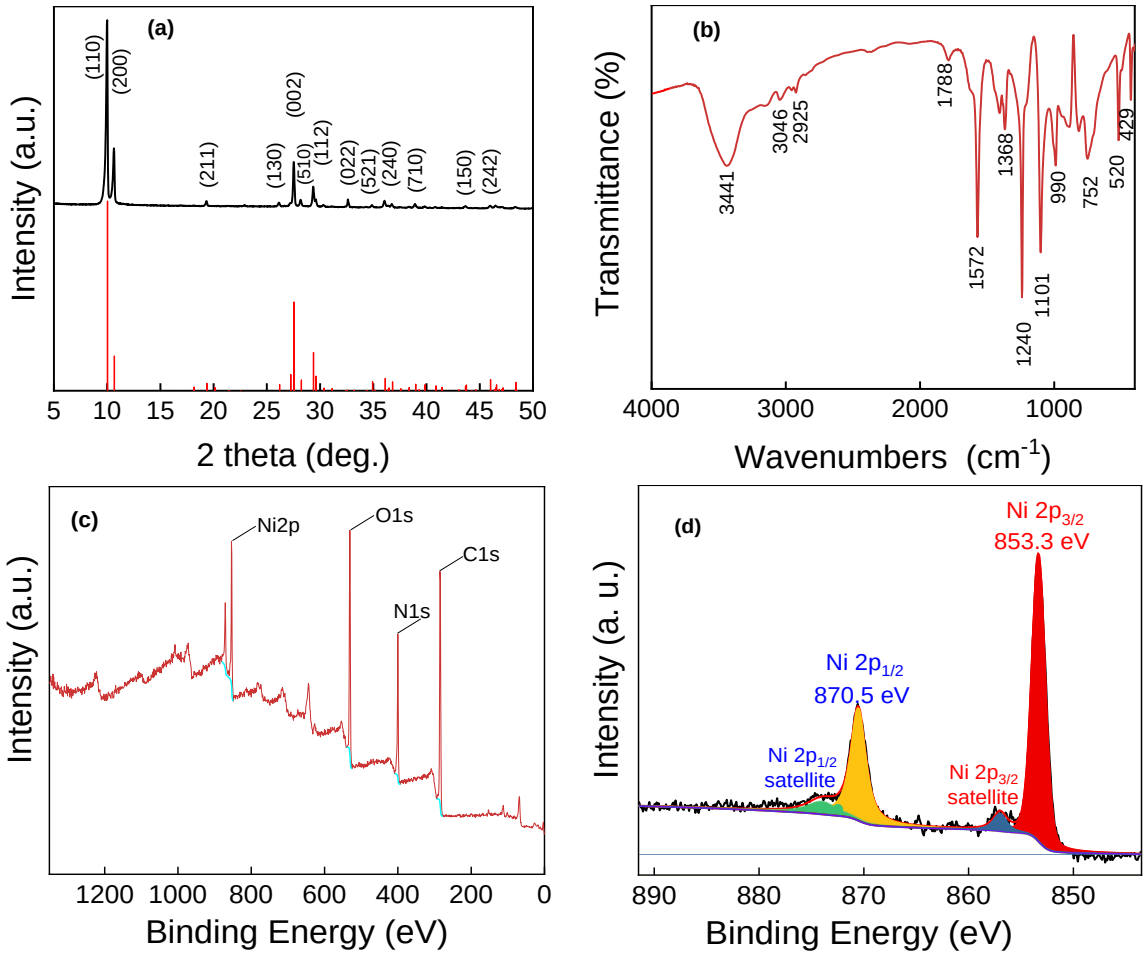

Figure 2. (**a**) XRD pattern, (**b**) FT-IR spectrum, (**c**) XPS survey spectrum and (**d**) Ni 2p XPS high-resolution spectra of the $Ni(DMG)_2$ complex.

The FT-IR spectrum of the $Ni(DMG)_2$ complex is shown in Figure 2b. The characteristic highest intensity absorption bands at 1240 and 1101 cm^{-1} observed in the sample can be attributed to the asymmetrical and symmetrical stretching vibrational modes of N–O. The strong absorption band at 1572 cm^{-1} can be assigned to the C=N stretching vibration mode of the sample [30,31], while the bands at 520 and 429 cm^{-1} can be attributed to the asymmetrical and symmetrical stretching vibrational modes of Ni–N [32,33]. The adsorption bands at 1368 and 990 cm^{-1} are attributed to the N–OH bond bending vibrational and N–O symmetric stretching vibrational models, respectively [32]. While the appearance of a band at 752 cm^{-1} is due to the C=N–O deformation vibration of the oxime group [34,35]. The broad absorption band at 3441 cm^{-1} is related to the O–H bonding stretching vibrational modes [32].

Furthermore, the weak band at 1788 cm^{-1} indicates a strong intramolecular hydrogen bonding in the $Ni(DMG)_2$ complex [36–39]. Also, the absorption bands related to asymmetrical and symmetrical stretching vibrational modes of C–H are observed around 3046 and 2925 cm^{-1}, respectively [40]. These results verified the formation of the $Ni(DMG)_2$ complex.

The surface elemental components and chemical state of the obtained $Ni(DMG)_2$ complex were characterized by XPS. The survey XPS spectra of the $Ni(DMG)_2$ complex are shown in Figure 2c. The calculation results show that the atomic percent rate of N, O, C, and Ni are about 18.21%, 20.00%, 58.26%, and 3.53% in the $Ni(DMG)_2$ complex, respectively. Thus, it can be confirmed that the $Ni(DMG)_2$ complex is of high purity. As shown in Figure 2d, the main characteristic peaks at 853.3 eV and 870.5 eV are assigned to Ni 2p3/2 and Ni 2p1/2, respectively. The peaks centered at 857.0 eV and 874.0 eV are the satellite peaks of Ni 2p3/2 and Ni 2p1/2, respectively. Meanwhile, the peak of Ni 2p1/2 at 870.5 eV also indicates the oxidation state of Ni in as-prepared samples is in the Ni^{2+} state [22]. This also further confirmed the formation of the $Ni(DMG)_2$.

2.2. Thermal Decomposition Behavior

To get a better understanding of thermal decomposition characteristics of the $Ni(DMG)_2$ complex, TG-DSC methods were adopted to study the thermal decomposition reaction behaviors of the $Ni(DMG)_2$ complex. TG and DSC curves for $Ni(DMG)_2$ complex at a heating rate of 10 °C·min^{-1} under a high purity argon atmosphere at a flow rate of 50 mL·min^{-1} are shown in Figure 3. One can see that the thermal decomposition reaction proceeds rapidly within the temperature range of 280–330 °C with a large exothermic effect. The sharp exothermic peak at 308.2 °C is observed in the DSC curve. The exothermic peak area is about 686.3 J·g^{-1}. The total mass loss is about 42.3%. The color of the solid residue after the thermal decomposition reaction is black. When the $Ni(DMG)_2$ completely decomposes, the theoretical value of mass loss for the formation of Ni or NiO is about 79.7% or 74.1%, respectively. This indicates that there are many other residual products, such as carbon formed in this decomposition process.

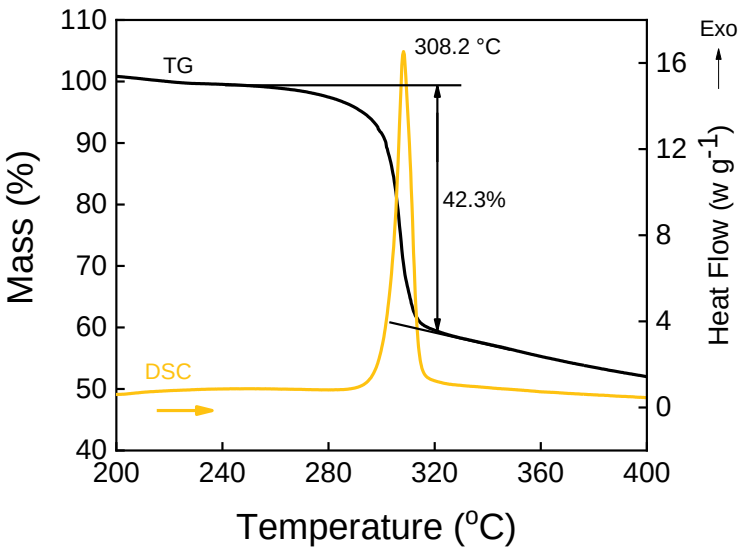

Figure 3. TG-DSC curves of the $Ni(DMG)_2$ complex.

To investigate the thermal decomposition mechanism of $Ni(DMG)_2$ complex, gas products released during the thermal decomposition of the $Ni(DMG)_2$ complex were detected simultaneously by mass spectra and FT-IR spectroscopy. The mass spectra of the principal gaseous products of $Ni(DMG)_2$ compound are shown in Figure 4a. It can be seen that the gas released from the $Ni(DMG)_2$ complex begins to appear at about 280 °C. The ion current number (m/z) of the major process products are 18, 17, 44, and 28, among which the ion current intensity of m/z = 18 is the highest. It is believed to be H_2O

as the dimethylglyoxime can undergo a dehydration reaction to produce a heterocyclic molecule [41]. The N–OH is also the weakest bond in the dimethylglyoxime molecule, so the H_2O forms very easily during the thermolysis of $Ni(DMG)_2$. The gas product with m/z = 17 could be NH_3. For the m/z of 44, two possible species are CO_2 or N_2O. The MS signals at m/z = 28, can be attributed to CO or N_2. It can also be seen that there are some weak ion currents of m/z = 12, 15, and 27 during the decomposition process, which indicate the existence of C, CH_3•, and HCN. The HCN may come from the reaction of NH_3 and C at high temperature.

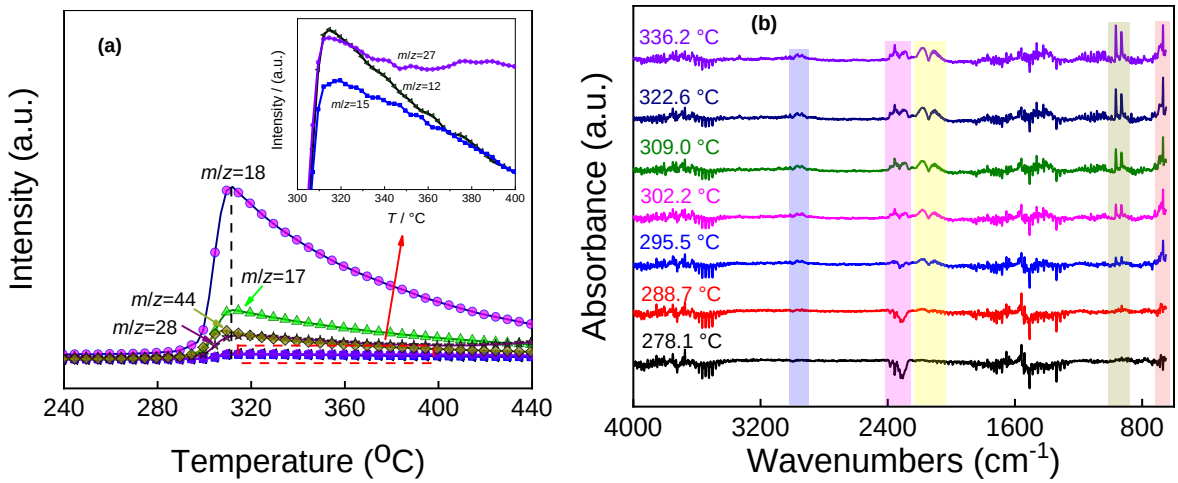

Figure 4. (**a**) MS and (**b**) FT-IR spectra of the evolved products released during the decomposition of $Ni(DMG)_2$ complex at different temperatures.

To further confirm the gaseous products of $Ni(DMG)_2$ complex, FT-IR spectroscopy was used. Figure 4b shows the FT-IR results of the main gaseous products at a different temperatures. Two significant changes in the FT-IR spectra can be found in the wavenumber region of 650–1000 cm^{-1} and 2000–2400 cm^{-1}. In the region between 650 and 1000 cm^{-1}, some new absorption peaks of gaseous products appear from 288.7 °C. An absorption peak at 668 cm^{-1} is attributed to the vibration of HCN, and the double peaks at 930 and 965 cm^{-1} are attributed to the vibrations of NH_3. Combined with the MS signals of m/z = 28 in Figure 4a, we can observe that the absorbance peaks at 2107 and 2185 cm^{-1} should be CO. Two bands at 2291 and 2355 cm^{-1} are assigned to CO_2 vibrations, which indicate that the MS signal of m/z = 44 in Figure 4a may be CO_2 [42]. However, NH_3 can be formed from the C=N bond only as a result of a reduction reaction, and the formation of CO_2 is the result of deep oxidation of the ligand. These reactions cannot occur simultaneously. Additionally, there is an excess of reducing elements in the $Ni(DMG)_2$ molecule and the formation of CO_2 during the thermolysis of $Ni(DMG)_2$ is unlikely. Most likely, this is atmospheric CO_2 or the oxidation product of $Ni(DMG)_2$ by air. So, the MS signal of m/z = 44 in Figure 4a must be N_2O. Generally, the characteristic absorption peak of N_2O is at about 2237 cm^{-1}, it can be affected by the absorption peak of CO_2 at 2291 cm^{-1}. Thus, N_2O is difficult to distinguish from the FT-IR results. According to Figure 4b, the peaks at 2939 and 2968 cm^{-1} are generally related to CH_3 vibrations, corresponding to m/z = 15 (Figure 4a. Therefore, by combining the results of the MS and FT-IR spectra, we can confirm that the main gaseous products of $Ni(DMG)_2$ complex are H_2O, NH_3, N_2O, CO, and HCN.

2.3. Non-Isothermal Decomposition Reaction Kinetics

Usually, the solid-state reaction rate ($d\alpha/dt$) can be described as:

$$\frac{d\alpha}{dt} = A\exp\left(-\frac{E}{RT}\right)f(\alpha) \quad (1)$$

where T is the temperature, α is the extent of conversion, A is the pre-exponential factor, t is the time, R is the gas constant, E is the activation energy, and $f(\alpha)$ is the reaction model. Some of the solid-state reaction kinetic models are listed in the literature [43].

Under the non-isothermal conditions, the experiments were carried out at a constant reaction rate ($\beta = \mathrm{d}T/\mathrm{d}t$). Then Equation (1) can be rearranged as follows:

$$\frac{\mathrm{d}\alpha}{\mathrm{d}T} = \frac{A}{\beta} f(\alpha) \exp\left(-\frac{E}{RT}\right) \tag{2}$$

The kinetic triplet, E, A, and $f(\alpha)$, is very important for kinetic studies, while it can be used to explain the reaction mechanism and make a kinetic prediction [44–46]. It is also the main aim of kinetic studies to obtain a kinetic triplet. The combined kinetic analysis method has been proved to be a promising method for determining the three kinetic parameters. It can determine all the kinetic parameters from the simultaneous treatment of experimental data, which can be obtained under any heating conditions [47–49]. In the combined kinetic analysis method, the reaction kinetic model can be described in the following general form:

$$f(\alpha) = c\alpha^m (1-\alpha)^n \tag{3}$$

This equation is commonly called the modified Šesták–Berggren empirical equation [50]. Equation (3) can acts as an umbrella. The most common physical models and their possible deviations from ideal conditions can be fitted by merely adjusting the parameters c, n, and m [47].

By substituting Equation (3) into Equation (2) and taking the logarithm, Equation (2) can be rearranged as the following equation:

$$\ln\left[\beta \frac{\mathrm{d}\alpha/\mathrm{d}T}{\alpha^m (1-\alpha)^n}\right] = \ln(cA) - \frac{E}{RT} \tag{4}$$

To obtain the parameters of Equation (4), one should simultaneously substitute the experiment data of α-T and ($\mathrm{d}\alpha/\mathrm{d}T$)-$T$ obtained at different heating rates. When the linear correlation coefficient (r) between the left-hand side of Equation (4) and the reciprocal temperature ($1/T$) reaches the maximum, the parameters c, n, and m can be obtained by the linear fitting method. Considering that the relative experimental errors of the kinetic data are larger at $\alpha < 0.1$ and $\alpha > 0.9$, only the data in the range of α = 0.1–0.9 were considered. Although the $f(\alpha)$ used in this method is an empirical kinetic equation, it does not have any previous assumption on the kinetic model of the reaction. It is very convenient to investigate the complex decomposition reactions, in which the $f(\alpha)$ estimated by experiment cannot match any ideal kinetic models.

Figure 5a shows the DSC curves of the $Ni(DMG)_2$ complex in N_2 flow at different linear heating rates of 5, 8, 10, and 12 °C·min^{-1}. The DSC parameters of $Ni(DMG)_2$ complex at different heating rates are listed in Table 1. It can be observed that the exothermic peaks are well-formed. According to Table 1, the onset, peak, and end temperatures (T_{onset}, T_{p}, and T_{end}) moved to high temperature with the increase of heating rate, respectively. The heat release (ΔQ) of the thermal decomposition process decreases with the increase of heating rate. The decomposition heat at a heating rate of 10 °C·min^{-1} is 1412 J·g^{-1}, and the decomposition peak temperature (309.2 °C) is very close to the TG-DSC result (peak temperature of 308.2 °C) in Figure 3 at the same heating rate.

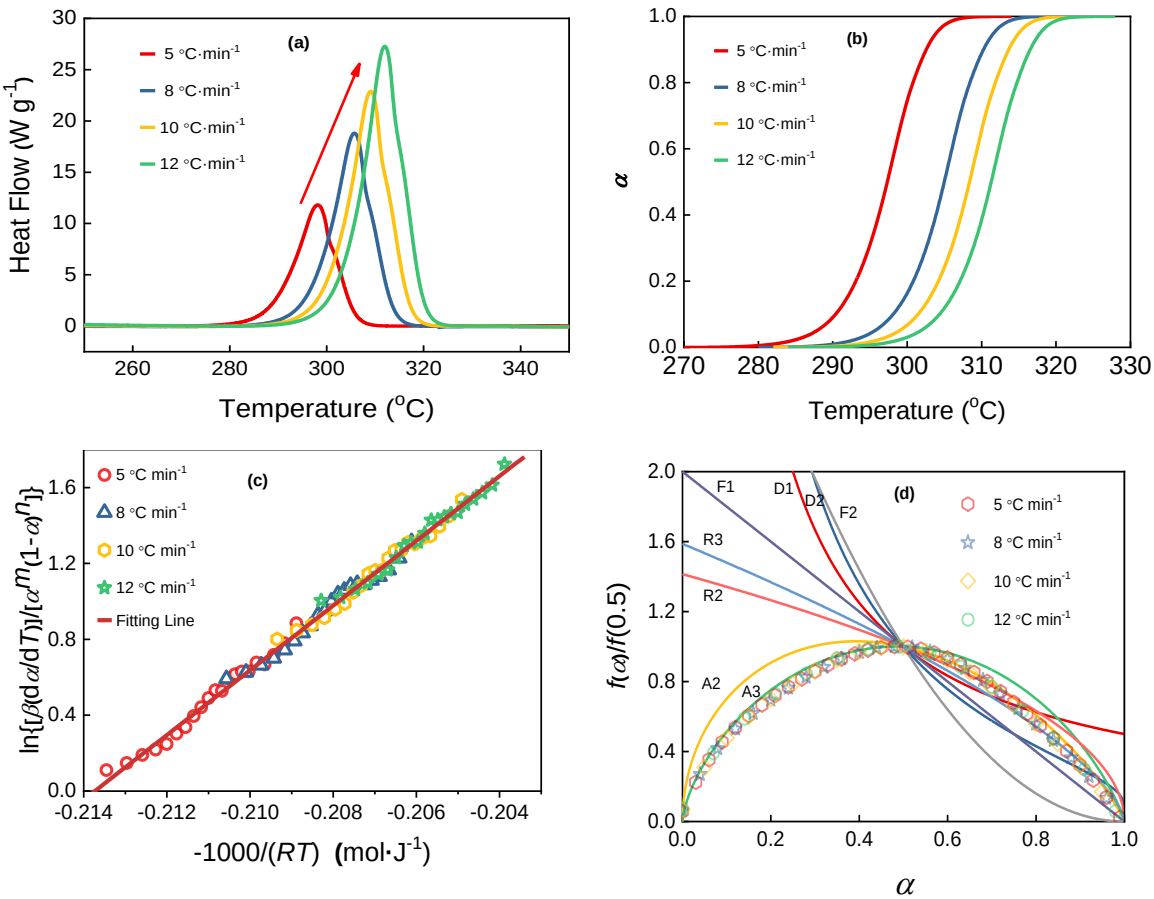

Figure 5. (**a**) DSC and (**b**) α–T curves of the $Ni(DMG)_2$ complex in N_2 flow at different heating rates of 5, 8, 10, and 12 °C·min^{-1}. (**c**) Combined kinetic analysis plots for non-isothermal decomposition data of $Ni(DMG)_2$ complex. (**d**) Comparison of the theoretical $f(\alpha)/f(0.5)$ curves (lines) corresponding to some of the ideal kinetic models with experimental $f(\alpha)/f(0.5)$ results (symbols) obtained by the combined kinetic analysis method.

Table 1. DSC parameters and combined kinetic analysis results of bis-(dimethylglyoximato) nickel(II) complex ($Ni(DMG)_2$) complex at different heating rates.

β/°C·min^{-1}	T_{onset}/°C	T_p/°C	T_{end}/°C	ΔQ/J·g^{-1}	Combined Kinetic Analysis				
					E/kJ·mol^{-1}	ln(cA/min^{-1})	m	n	r
5	289.2	298.2	303.5	1473	170.61 ± 0.65	36.46 ± 0.13	0.860	1.009	0.9977
8	297.0	305.7	311.2	1451					
10	300.5	309.2	314.5	1412					
12	303.6	312.0	313.8	1398					

The corresponding non-isothermal conversion (α–T) curves for the thermal decomposition process of $Ni(DMG)_2$ complex at the different heating rates are shown in Figure 5b. It can be seen that all α–T curves have a sigmoidal character, and they are moved to higher temperature with the heating rate increase. The α–T data, in the range of $0.1 < \alpha < 0.9$, were subjected to combined kinetic analysis studies for determining the kinetic parameters of the reaction. Figure 5c shows the calculation results of the reaction by the combined kinetic analysis method through the plot of the left-hand side of Equation (4) versus $1/T$. The kinetic parameters obtained by the combined kinetic analysis methods are also summarized in Table 1. As it can seen, the experimental data in the range of α fit closely to a straight line, the linear correlation coefficient (r) can achieve 0.9977 for the fitting parameters n = 0.860 and m =1.009. The activation energy and ln(cA) obtained from the slope and intercept of the fitting line are 170.61 ± 0.65 kJ·mol^{-1} and 36.46 ± 0.13, respectively.

To further confirm the possible reaction mechanism functions, the differential master plot method, which is defined by Equation (5), can be applied [51]. Figure 5d shows the theoretical $f(\alpha)/f(0.5)$ curves for different models (lines), and four experimental $f(\alpha)/f(0.5)$ results (symbols) obtained by using Equation (5). It can be seen from Figure 5d that the experimental $f(\alpha)/f(0.5)$ results at different heating rates are not in good agreement with any one of the theoretical $f(\alpha)/f(0.5)$ curves. However, it should be noted that the experimental curve is in partial agreement with random nucleation and 3D growth of nuclei (A3) model in the range of $\alpha < 0.5$ and random nucleation and 2D growth of nuclei (A2) model in the range of $\alpha > 0.5$. This may indicate that the decomposition process of $Ni(DMG)_2$ complex is controlled by two processes. In the initial decomposition process, it follows the random nucleation and 3D growth of the nuclei model. As the reaction proceeds, the decomposition process gradually shifts to the 2D growth of the nuclei model.

$$\frac{f(\alpha)}{f(0.5)} = \frac{\left(\frac{d\alpha}{dT}\right)_{\alpha}}{\left(\frac{d\alpha}{dT}\right)_{\alpha=0.5}} \frac{\exp\left(\frac{E}{RT_{\alpha}}\right)}{\exp\left(\frac{E}{RT_{\alpha=0.5}}\right)} \tag{5}$$

Generally, the dependence of apparent activation energy (E_α) on α, obtained by the isoconversional methods, is important for distinguishing and treating the multistep reaction kinetics. A significant variation of E_α-α indicates that the reaction process is kinetically complex, and one cannot apply any one of the ideal kinetic models to describe a possible reaction mechanism of such a process throughout the whole range of experimental conversions and temperatures [43]. To obtain the dependence of E_α-α, the integral isoconversional method developed by Vyazovkin [52–54] was used. For a series of runs performed at different heating rates, the E_α value can be determined by minimizing the following function [52]:

$$\Phi(E_\alpha) = \sum_{i=1}^{n} \sum_{j \neq i}^{n} \frac{I(E_\alpha, T_{\alpha,i})\beta_j}{I\left(E_\alpha, T_{\alpha,j}\right)\beta_i} \tag{6}$$

where the temperature integral

$$I(E_\alpha, T_{\alpha,i}) = \int_{T_0}^{T_\alpha} \exp\left(-\frac{E_\alpha}{RT}\right) dT \tag{7}$$

is solved numerically using the Runge–Kutta method. Then the dependence of E_α on α can be obtained by minimizing the $\Phi(E_\alpha)$ function repeatedly for each value of α.

Figure 6 shows the dependence of E_α on α obtained by the Vyazovkin method for the thermal decomposition of $Ni(DMG)_2$ complex. It indicates that the activation energy of the decomposition process has significantly changed at high and low conversions. The reason is that the relative experimental errors of the kinetic data are larger at $\alpha < 0.1$ and $\alpha > 0.9$. The average activation energy is 167.80 ± 1.49 kJ mol^{-1} in the range of $0.1 \leq \alpha \leq 0.9$, which is almost identical to the result obtained by the combined kinetic analysis method. Also note that, the change of E_α in the range of $0.1 < \alpha < 0.6$ was significantly greater than the $0.6 < \alpha < 0.9$. This indicates that the thermal decomposition process of $Ni(DMG)_2$ complex was a complex multistep reaction, so it is extremely difficult to properly evaluate the reaction mechanism by the ideal kinetic model.

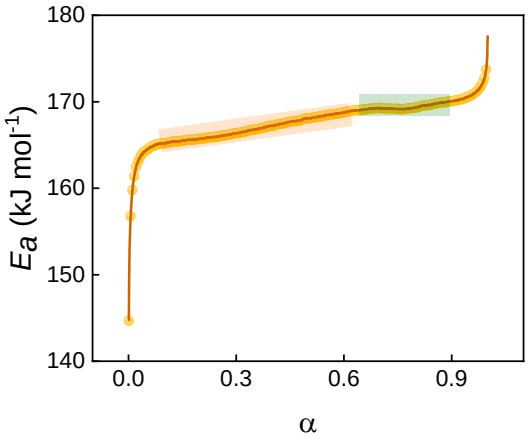

Figure 6. E_α-α curve for the thermal decomposition of $Ni(DMG)_2$ complex.

3. Experimental

3.1. Materials

Dimethylglyoxime (DMG), nickel chloride hexahydrate ($NiCl_2{\cdot}6H_2O$), and absolute ethanol were all obtained from the Aladdin Chemical Reagent Co., Ltd. (Shanghai, China). All of the chemical reagents were analytical grade, commercially available and used without purification further.

3.2. Synthesis of $Ni(DMG)_2$

An amount of 100 mL absolute ethanol was mixed with 1.0015 g dimethylglyoxime (DMG) and 1.0303 g nickel chloride hexahydrate ($NiCl_2{\cdot}6H_2O$), followed by stirring until completely dissolved. The mixed solution was poured into a round bottom flask and the pH adjusted of the solution to pH 8. Then the solution was heated and stirred at 85 °C for 30 min, and reacted for 2 h at 55 °C with no agitation. The obtained precipitate was washed with ethanol. The obtained red precipitate was $Ni(DMG)_2$. Finally, the dried sample was heated at 400 °C for 2 h and kept in an argon atmosphere. Elemental analysis (%), calculated for $Ni(DMG)_2$ ($C_8H_{14}N_4O_4Ni$, 288.91): C (33.26%), H (4.88%), N (19.39%); found: C (33.64%), H (4.98%), N (19.22%). The chemical structure of $Ni(DMG)_2$ is shown in Figure 1a.

3.3. Apparatus and Measurements

Field-emission environment scanning electron microscope (SEM, FEI Quanta 600, Hillsboro, OR, USA) was used to characterize the morphology of the sample. Energy-dispersive X-ray spectroscopy (EDS, OXFORD INCA Penta FET × 3) was used to roughly examine the composition, which was attached with SEM.

The phase structure and purity of the $Ni(DMG)_2$ were confirmed by powder X-ray diffraction (XRD, PANalytical X'Pert PRO, Amsterdam, Netherlands). The radiation source of the X-ray powder Diffractometer is Cu K_α (λ = 1.5418 Å) at 40 kV and 40 mA. The testing temperature was ambient temperature, and the range of 2θ was 5° to 90° with steps of 0.05°.

A Fourier Transform Infrared (FT-IR, Bruker Tensor 27, Karlsruhe, Germany) spectrometer was used to record the infrared spectra. The samples were pressed into pellets. The mass ratio of KBr pellets with KBr to sample was approximately 30:1. The spectral range was 4000–400 cm^{-1} with a resolution of 4 cm^{-1}.

The information of element composition was obtained by X-ray photoelectron spectroscopy (XPS, NEXSA, Thermo scientific, Waltham, MA, USA) instrument and the radiation source was Al K_α (1468.68 eV). The binding energy of the C1s peak at 284.6 eV was used to calibrate the obtained XPS peaks.

The thermal decomposition behavior and kinetic analysis of the sample were investigated by differential scanning calorimetry (DSC). A NETZSCH DSC204 instrument (Selb, Bavaria, Germany) equipped with a water-cooling system which was used to carry out the DSC measurement. The instrument was calibrated by an indium standard. In this work, the mass of each sample was about 1.0 mg. The test temperature range was room temperature to 500 °C. The heating rates were 5.0, 8.0, 10.0, and 12.0 °C·min^{-1}. The carrier gas was nitrogen at a flow rate of 50 mL·min^{-1}.

Thermal decomposition and evolved gas analysis of $Ni(DMG)_2$ were performed using thermogravimetric analysis, differential scanning calorimetry, Fourier transform infrared spectrometer and mass spectrometer (TG-DSC-FTIR-MS) coupling technique with a STA449C thermal analyzer (NETZSCH, Selb, Bavaria, Germany), a QMS-403C mass spectrometer (NETZSCH, Selb, Bavaria, Germany), and a 5700 infrared spectrometer (Nicolet, Madison, WI, USA). The thermal decomposition measurements were performed under a high purity argon atmosphere at a flow rate of 50 mL·min^{-1}. The test temperature range was 30 to 500 °C, and the heating rate was 10 °C·min^{-1}. The sample mass was about 2.0 mg. The transfer tubes were used to directly transfer the evolved gases during the thermal decomposition process, and finally detected by MS and FT-IR.

4. Conclusions

As a potential combustion catalyst, the fiber-like $Ni(DMG)_2$ complex was successfully synthesized and characterized by SEM-EDS, FT-IR, XRD, and XPS. The thermal decomposition behavior and gaseous products of the $Ni(DMG)_2$ complex were characterized by TG-DSC-FTIR-MS techniques. The decomposition reaction of $Ni(DMG)_2$ occurs in the temperature range 280–330 °C with a large exothermic effect. The experimental total mass loss during the thermal decomposition of $Ni(DMG)_2$ is lower than the theoretical value of complete decomposition. The gas products released during the thermal decomposition were detected simultaneously by MS and FT-IR, and the results show that the main gas products are H_2O, NH_3, N_2O, CO, and HCN. The ion current intensity of H_2O (m/z = 18) is the highest according to the MS results.

The non-isothermal decomposition reaction kinetic parameters were obtained by both isoconversional Vyazovkin methods and the combined kinetic analysis method. The activation energy obtained by the combined kinetic analysis method was 170.61 ± 0.65 kJ·mol^{-1}, which is almost the same as that obtained by the isoconversional Vyazovkin method. The initial decomposition process follows the random nucleation and three-dimensional growth of the nuclei model. As the reaction proceeds, the decomposition process gradually shifts to the two-dimensional growth of the nuclei model. The dependence of E_α on α obtained by the Vyazovkin method also indicates that the thermal decomposition process is a complex multistep reaction.

Author Contributions: Conceptualization, E.Y., S.X., and F.Z.; methodology, E.Y. and T.H.; formal analysis, N.Z., J.Y., and Y.Y.; investigation, E.Y. S.X., and T.H.; data curation, C.W.; writing—original draft preparation, E.Y.; writing—review and editing, H.L. and F.Z.; supervision, F.Z. All authors have read and agreed to the published version of the manuscript.

Funding: This research was supported by the National Natural Science Foundation of China (No. 21473130).

Conflicts of Interest: The authors declare no conflict of interest.

References

1. Yi, J.; Zhao, F.; Wang, B.; Liu, Q.; Zhou, C.; Hu, R.; Ren, Y.; Xu, S.; Xu, K.; Ren, X. Thermal behaviors, nonisothermal decomposition reaction kinetics, thermal safety and burning rates of BTATz-CMDB propellant. *J. Hazard. Mater.* **2010**, *181*, 432–439. [CrossRef] [PubMed]
2. Wang, Y.; Zhao, F.; Ji, Y.; Yi, J.; An, T.; Liu, W. Synthesis, crystal structure and thermal behavior of 4-amino-3,5-dinitropyrazole copper salt. *Chin. Chem. Lett.* **2014**, *25*, 902–906. [CrossRef]
3. Gao, J.; Wang, L.; Yu, H.; Xiao, A.; Ding, W. Recent research progress in burning rate catalysts. *Propellants Explos. Pyrotech.* **2011**, *36*, 404–409. [CrossRef]

4. Zhao, N.; Li, J.; Gong, H.; An, T.; Zhao, F.; Yang, A.; Hu, R.; Ma, H. Effects of α-Fe_2O_3 nanoparticles on the thermal behavior and non-isothermal decomposition kinetics of nitrocellulose. *J. Anal. Appl. Pyrolysis* **2016**, *120*, 165–173. [CrossRef]
5. Pei, J.; Zhao, F.; Song, X.; Ren, X.; Gao, H.; An, T.; An, J.; Hu, R. Effects of nano-CuO particles on thermal decomposition behavior and decomposition mechanism of BAMO–GAP copolymer. *J. Anal. Appl. Pyrolysis* **2015**, *112*, 88–93. [CrossRef]
6. Patil, P.R.; Krishnamurthy, V.N.; Joshi, S.S. Effect of nano-copper oxide and copper chromite on the thermal decomposition of ammonium perchlorate. *Propellants Explos. Pyrotech.* **2008**, *33*, 266–270. [CrossRef]
7. Mahinroosta, M. Catalytic effect of commercial nano-CuO and nano-Fe_2O_3 on thermal decomposition of ammonium perchlorate. *J. Nanostruct. Chem.* **2013**, *3*, 47. [CrossRef]
8. Budhwar, A.S.; Gautam, A.; More, P.V.; Pant, C.S.; Banerjee, S.; Khanna, P.K. Modified iron oxide nanoparticles as burn rate enhancer in composite solid propellants. *Vacuum* **2018**, *156*, 483–491. [CrossRef]
9. Hao, G.; Liu, J.; Xiao, L.; Gao, H.; Qiao, Y.; Jiang, W.; Zhao, F.; Gao, H. Effect of drying methods on catalytic performance of nano-sized copper β-resorcylate. *J. Therm. Anal. Calorim.* **2016**, *124*, 1367–1374. [CrossRef]
10. Zhao, W.; Zhang, T.; Song, N.; Zhang, L.; Chen, Z.; Yang, L.; Zhou, Z. Assembly of composites into a core–shell structure using ultrasonic spray drying and catalytic application in the thermal decomposition of ammonium perchlorate. *RSC Adv.* **2016**, *6*, 71223–71231. [CrossRef]
11. Liu, J.; Qiu, H.; Han, J.; Yang, L. Synthesis of energetic complexes $[Co(en)(H_2BTI)_2]_2 \cdot en$, $[Cu_2(en)_2(HBTI)_2]_2$ and catalytic study on thermal decomposition of ammonium perchlorate. *Propellants Explos. Pyrotech.* **2019**, *4*, 816–820. [CrossRef]
12. Yuan, Z.; Zhao, F.; Yang, Y.; Song, X.; Gao, H.; Xu, S. Comparative investigation of different nano-metal materials on combustion properties of DB and CMDB propellants. *Int. J. Energetic Mater. Chem. Propuls.* **2017**, *16*, 219–229. [CrossRef]
13. Pang, W.; De Luca, L.T.; Fan, X.; Maggi, F.; Xu, H.; Xie, W.; Shi, X. Effects of different nano-sized metal oxide catalysts on the properties of composite solid propellants. *Combust. Sci. Technol.* **2016**, *188*, 315–328. [CrossRef]
14. Pang, W.; Fan, X.; Zhao, F.; Zhang, W.; Xu, H.; Yu, H.; Xie, W.; Yan, N.; Liu, F. Effects of different nano-metric particles on the properties of composite solid propellants. *Propellants Explos. Pyrotech.* **2014**, *39*, 329–336. [CrossRef]
15. Sharma, J.K.; Srivastava, P.; Singh, G.; Akhtar, M.S.; Ameen, S. Biosynthesized NiO nanoparticles: Potential catalyst for ammonium perchlorate and composite solid propellants. *Ceram. Int.* **2015**, *41*, 1573–1578. [CrossRef]
16. Liu, X.; Zhao, D.; Bi, F.; Fan, X.; Zhao, F.; Zhang, G.; Zhang, W.; Gao, Z. Synthesis, characterization, migration studies and combustion catalytic performances of energetic ionic binuclear ferrocene compounds. *J. Organomet. Chem.* **2014**, *762*, 1–8. [CrossRef]
17. Patra, S.G.; Mandal, N.; Datta, A.; Datta, D. On bonding in bis(dimethylglyoximato)nickel(II). *Comput. Theor. Chem.* **2017**, *1114*, 118–124. [CrossRef]
18. Rath, M.; Behera, L.P.; Dash, B.; Sheik, A.R.; Sanjay, K. Recovery of dimethylglyoxime (DMG) from Ni-DMG complexes. *Hydrometallurgy* **2018**, *176*, 229–234. [CrossRef]
19. Farhadi, S.; Kazem, M.; Siadatnasab, F. NiO nanoparticles prepared via thermal decomposition of the bis(dimethylglyoximato)nickel(II) complex: A novel reusable heterogeneous catalyst for fast and efficient microwave-assisted reduction of nitroarenes with ethanol. *Polyhedron* **2011**, *30*, 606–613. [CrossRef]
20. Pang, H.; Lu, Q.; Li, Y.; Gao, F. Facile synthesis of nickel oxide nanotubes and their antibacterial, electrochemical and magnetic properties. *Chem. Commun.* **2009**, 7542–7544. [CrossRef]
21. Li, X.; Zhang, X.; Li, Z.; Qian, Y. Synthesis and characteristics of NiO nanoparticles by thermal decomposition of nickel dimethylglyoximate rods. *Solid State Commun.* **2006**, *137*, 581–584. [CrossRef]
22. Sarkar, B.; Kwek, W.; Verma, D.; Kim, J. Effective vacuum residue upgrading using sacrificial nickel(II) dimethylglyoxime complex in supercritical methanol. *Appl. Catal. A* **2017**, *545*, 148–158. [CrossRef]
23. Dakhel, A.A.; Ali-Mohamed Ahmed, Y. Electrical properties of thermally evaporated nickel-dimethylglyoxime thin films. *J. Phys. Chem. Solids* **2005**, *66*, 1080–1084. [CrossRef]
24. Dakhel, A.A.; Ali-Mohamed Ahmed, Y.; Henari, F.Z. Structural and optical studies of evaporated bis-(dimethylglyoximato)nickel(II) thin films. *Opt. Mater.* **2006**, *28*, 925–929. [CrossRef]

25. Takeda, K.; Hayashi, J.; Shirotani, I.; Fukuda, H.; Yakushi, K. Structural, optical, and electrical properties of one-dimensional bis(dimethylglyoximato)nickel(ii), $Ni(dmg)_2$ at high pressure. *Mol. Cryst. Liq. Cryst.* **2006**, *460*, 131–144. [CrossRef]
26. Godycki, L.E.; Rundle, R.E. The structure of nickel dimethylglyoxime. *Acta Crystallogr.* **1953**, *6*, 487–495. [CrossRef]
27. Williams, D.E.; Wohlauer, G.; Rundle, R.E. Crystal structures of nickel and palladium dimethylglyoximes. *J. Am. Chem. Soc.* **1959**, *81*, 755–756. [CrossRef]
28. Li, D.; Xu, D.; Xu, Y. Redetermination of bis(dimethylglyoximato-k^2N,N')nickel(II). *Acta Crystallogr. Sect. E Struct. Rep. Online* **2003**, *59*, m1094–m1095. [CrossRef]
29. Bruce-Smith, I.F.; Zakharov, B.A.; Stare, J.; Boldyreva, E.V.; Pulham, C.R. Structural properties of nickel dimethylglyoxime at high pressure: Single-crystal X-ray diffraction and DFT studies. *J. Phys. Chem. C* **2014**, *118*, 24705–24713. [CrossRef]
30. Xavier, K.O.; Chacko, J.; Mohammed Yusuff, K.K. Zeolite-encapsulated Co(II), Ni(II) and Cu(II) complexes as catalysts for partial oxidation of benzyl alcohol and ethylbenzene. *Appl. Catal. A* **2004**, *258*, 251–259. [CrossRef]
31. Coropceanu, E.; Rudic, V.; Cepoi, L.; Rudi, L.; Lozan, V.; Chiriac, T.; Miscu, V.; Bulhac, I.; Kravtsov, V.; Bourosh, P. Synthesis and crystal structure of $[Co(DmgH)_2(Thio)_2]_2F[PF_6]$. The effect of fluorine-containing Co(III) dioximates on the physiological processes of the microalga porphyridium cruentum. *Russ. J. Coord. Chem.* **2019**, *45*, 200–207. [CrossRef]
32. Yang, B.; Li, J.; Zhang, L.; Xu, G. A molecularly imprinted electrochemiluminescence sensor based on the mimetic enzyme catalytic effect for ultra-trace Ni^{2+} determination. *Analyst* **2016**, *141*, 5822–5828. [CrossRef] [PubMed]
33. Szabó, A.; Kovács, A. Vibrational analysis of the bis(dimethylglyoximato)nickel(II) complex. *J. Mol. Struct.* **2003**, *651–653*, 547–553. [CrossRef]
34. Adkhis, A.; Djebbar, S.; Benali-Baïtich, O.; Kadri, A.; Khan, M.A.; Bouet, G. Synthesis, characterization, and electrochemical behavior of mixed-ligand complexes of Cobalt(III) with dimethylglyoxime and some amino acids. *Synth. React. Inorg. Met. Org. Chem.* **2003**, *33*, 35–50. [CrossRef]
35. Saxena, V.K.; Gupta, M.; Srivastava, M.N. Synthesis and characterization of complexes of Copper(II), Nickel(II), Cobalt(II) and Zinc(II) with histidine and glycine or alanine. *Synth. React. Inorg. Met. Org. Chem.* **1996**, *26*, 1661–1676. [CrossRef]
36. Ponnuswamy, T.; Chyan, O. Detection of Ni^{2+} by a dimethylglyoxime probe using attenuated total-reflection infrared spectroscopy. *Anal. Sci.* **2002**, *18*, 449–453. [CrossRef] [PubMed]
37. Caleb Noble Chandar, S.; Sangeetha, D.; Arumugham, M.N. Synthesis, structure, CMC values, thermodynamics of micellization, steady-state photolysis and biological activities of hexadecylamine cobalt(III) dimethyl glyoximato complexes. *Transit. Met. Chem.* **2011**, *36*, 211–216. [CrossRef]
38. Salih, B.M.M.; Satyanarayana, S. Vitamin B12 models: Synthesis and characterization of cyano bridged dicobaloximes and antimicrobial activity. *Afr. J. Pure Appl. Chem.* **2009**, *3*, 170–176.
39. Cardoso, W.S.; Dias, V.L.N.; Costa, W.M.; de Araujo Rodrigues, I.; Marques, E.P.; Sousa, A.G.; Boaventura, J.; Bezerra, C.W.B.; Song, C.; Liu, H.; et al. Nickel-dimethylglyoxime complex modified graphite and carbon paste electrodes: Preparation and catalytic activity towards methanol/ethanol oxidation. *J. Appl. Electrochem.* **2009**, *39*, 55–64. [CrossRef]
40. Panja, P.K.; Bala, S.; Pal, C.; Ghosh, P.N. Infrared spectroscopic studies of dimethylglyoxime chelates of nickel, cobalt, copper, palladium and platinum. *J. Mol. Struct.* **1991**, *249*, 277–283. [CrossRef]
41. Toma, H.E.; Morino, L.A. Thermal decomposition of bis(dimethylglyoximate) iron(II) complexes containing axial *N*-heterocyclic ligands. *J. Therm. Anal.* **1990**, *36*, 7–15. [CrossRef]
42. Ding, L.; Zhao, F.; Pan, Q.; Xu, H. Research on the thermal decomposition behavior of NEPE propellant containing CL-20. *J. Anal. Appl. Pyrolysis* **2016**, *121*, 121–127. [CrossRef]
43. Vyazovkin, S.; Burnham, A.K.; Criado, J.M.; Pérez-Maqueda, L.A.; Popescu, C.; Sbirrazzuoli, N. ICTAC Kinetics Committee recommendations for performing kinetic computations on thermal analysis data. *Thermochim. Acta* **2011**, *520*, 1–19. [CrossRef]
44. Tan, G.; Wang, Q.; Zheng, H.; Zhao, W.; Zhang, S.; Liu, Z. Concept of variable activation energy and its validity in nonisothermal kinetics. *J. Phys. Chem. A* **2011**, *115*, 5517–5524. [CrossRef]

45. Zhou, D.; Grant, D.J.W. Model Dependence of the activation energy derived from nonisothermal kinetic data. *J. Phys. Chem. A* **2004**, *108*, 4239–4246. [CrossRef]
46. Maraii, D.; Farjas, J.; Fontrodona, X.; Dammak, M. Synthesis, structural study, thermal, optical properties and characterization of the new compound $[C_6H_7N_2O_2]_3TeCl_5{\cdot}2Cl$. *Chin. Chem. Lett.* **2017**, *28*, 1773–1779. [CrossRef]
47. Pérez-Maqueda, L.A.; Criado, J.M.; Sánchez-Jiménez, P.E. Combined kinetic analysis of solid-state reactions: A powerful tool for the simultaneous determination of kinetic parameters and the kinetic model without previous assumptions on the reaction mechanism. *J. Phys. Chem. A* **2006**, *110*, 12456–12462. [CrossRef]
48. Sánchez-Jiménez, P.E.; Pérez-Maqueda, L.A.; Perejón, A.; Criado, J.M. Combined kinetic analysis of thermal degradation of polymeric materials under any thermal pathway. *Polym. Degrad. Stab.* **2009**, *94*, 2079–2085. [CrossRef]
49. García-Garrido, C.; Pérez-Maqueda, L.A.; Criado, J.M.; Sánchez-Jiménez, P.E. Combined kinetic analysis of multistep processes of thermal decomposition of polydimethylsiloxane silicone. *Polymer* **2018**, *153*, 558–564. [CrossRef]
50. Šesták, J.; Berggren, G. Study of the kinetics of the mechanism of solid-state reactions at increasing temperatures. *Thermochim. Acta* **1971**, *3*, 1–12. [CrossRef]
51. Gotor, F.J.; Criado, J.M.; Malek, J.; Koga, N. Kinetic analysis of solid-state reactions: The universality of master plots for analyzing isothermal and nonisothermal experiments. *J. Phys. Chem. A* **2000**, *104*, 10777–10782. [CrossRef]
52. Vyazovkin, S.; Dollimore, D. Linear and nonlinear procedures in isoconversional computations of the activation energy of nonisothermal reactions in solids. *J. Chem. Inf. Comput. Sci.* **1996**, *36*, 42–45. [CrossRef]
53. Vyazovkin, S. Evaluation of activation energy of thermally stimulated solid-state reactions under arbitrary variation of temperature. *J. Comput. Chem.* **1997**, *18*, 393–402. [CrossRef]
54. Vyazovkin, S. Modification of the integral isoconversional method to account for variation in the activation energy. *J. Comput. Chem.* **2001**, *22*, 178–183. [CrossRef]

© 2020 by the authors. Licensee MDPI, Basel, Switzerland. This article is an open access article distributed under the terms and conditions of the Creative Commons Attribution (CC BY) license (http://creativecommons.org/licenses/by/4.0/).